Role of forest regrowth in global carbon sink dynamics

Pugh, Thomas; Lindeskog, Mats; Smith, Benjamin; Poulter, Benjamin; Arneth, Almut; Haverd, Vanessa; Calle, Leonardo

DOI:
10.1073/pnas.1810512116

The role of forest regrowth in global carbon sink dynamics

Thomas A.M. Pugh[a,b], Mats Lindeskog[c], Benjamin Smith[c,d], Benjamin Poulter[e,f], Almut Arneth[g], Vanessa Haverd[h] and Leonardo Calle[e]

[a] School of Geography, Earth and Environmental Sciences, University of Birmingham, Birmingham, B15 2TT, United Kingdom.
[b] Birmingham Institute of Forest Research, University of Birmingham, Birmingham, B15 2TT, United Kingdom.
[c] Department of Physical Geography and Ecosystem Science, Lund University, 22362 Lund, Sweden.
[d] Hawkesbury Institute for the Environment, Western Sydney University, Locked Bag 1797, Penrith, NSW 2751, Australia,
[e] Department of Ecology, Montana State University, Bozeman, Montana 59717, USA.
[f] Biospheric Sciences Laboratory, NASA Goddard Space Flight Center, Greenbelt, MD 20771
[g] Karlsruhe Institute of Technology, Institute of Atmospheric Environmental Research (IMK-IFU), Kreuzeckbahnstrasse 19, 82467, Garmisch-Partenkirchen, Germany.
[h] CSIRO Marine and Atmospheric Research, GPO Box 1700, Canberra ACT 2601, Australia.

Corresponding author: Thomas A.M. Pugh, t.a.m.pugh@bham.ac.uk

ORCIDs:
Thomas A.M. Pugh, 0000-0002-6242-7371

Classification: BIOLOGICAL SCIENCES (ENVIRONMENTAL SCIENCES)

Keywords: Forest; Carbon sink; Regrowth

Abstract

Although the existence of a large carbon sink in terrestrial ecosystems is well-established, the drivers of this sink remain uncertain. It has been suggested that perturbations to forest demography caused by past land-use change, management and natural disturbances may be causing a large component of current carbon uptake. Here we use a global compilation of forest age observations, combined with a terrestrial biosphere model with explicit modelling of forest regrowth, to partition the global forest carbon sink between old-growth and regrowth stands over the period 1981-2010. For 2001-2010 we find a carbon sink of 0.85 (0.66-0.96) Pg yr^{-1} located in intact old-growth forest, primarily in the moist tropics and boreal Siberia, and 1.30 (1.03-1.96) Pg yr^{-1} located in stands regrowing after past disturbance. Approaching half of the sink in regrowth stands would have occurred from demographic changes alone, in the absence of other environmental changes. These age-constrained results show consistency with those simulated using an ensemble of demographically-enabled terrestrial biosphere models following an independent reconstruction of historical land-use and management. We estimate that forests will accumulate an additional 69 (44-131) Pg C in live biomass from changes in demography alone if natural disturbances, wood harvest and reforestation continue at rates comparable to those during 1981-2010. Our results confirm that it is not possible to understand the current global terrestrial carbon sink without accounting for the sizeable sink due to forest demography. They also imply that a large portion of the current terrestrial carbon sink is strictly transient in nature.

Significance Statement

Regrowth of forests following past disturbances is expected to be an important driver behind the large uptake of anthropogenic CO_2 emissions by the terrestrial biosphere. Yet estimates of the size of this uptake vary widely. We combined independent observation-based and model-based sources of disturbance history information to calculate the carbon sink in regrowth forests. On-going carbon uptake due to forest demography is large, but much smaller than previous influential estimates have suggested. Contrary to previous findings, these latest data sources indicate that the sink is predominantly in mid-high latitude, rather than tropical, forests. The remaining uptake potential in forest biomass under current disturbance rates is equivalent to seven years of emissions from fossil fuel burning at 2016 levels.

\body

The terrestrial biosphere is believed to have provided a net sink for approximately 20% of carbon dioxide emitted by fossil fuel burning and industry over the last three decades (1), with the majority estimated to occur in forests (2). Forests are thus believed to retard anthropogenic climate change by slowing the rate of carbon dioxide (CO_2) accumulation in the atmosphere. However, the drivers and geographical distribution of this sink remain poorly characterized, limiting both our understanding of both why it occurs and our ability to predict its continued future existence.

Globally, forests sequester large amounts of carbon in woody biomass and soils. Theoretically, in a forest that is in pseudo-equilibrium with its environment, biomass growth will be balanced by turnover, and litter inputs from biomass turnover by heterotrophic respiration, such that, in the long-term average over a forest landscape, carbon stored in the ecosystem will remain relatively constant (3, 4). But even in pseudo-equilibrium systems, external perturbations can temporarily stimulate biomass growth relative to heterotrophic respiration, or vice versa, and it is questionable whether a true equilibrium is ever achieved in practice (4). One such potential, anthropogenic, perturbation is the fertilizing effect of elevated atmospheric CO_2 concentrations on photosynthesis, which may stimulate woody biomass growth. This process is widely believed to lie behind the stimulation in growth observed in old-growth forest stands (5, 6), and has been estimated to account for 60% of the land carbon sink implied by the balance of change in atmospheric and oceanic stocks and emissions (7). Another perturbation is a shift in forest age towards younger forests occurring as a result of historical peaks in tree mortality, due, for instance, to intensive forest harvesting, changes in natural disturbance regimes, or reestablishment of forest stands on previously non-forested land, such as on abandoned agricultural land. Such a shift of forest age away from the theoretical system equilibrium can be expected to lead to increased net primary production, reduced biomass turnover rates from tree death, and changes in soil and litter stocks as a result of the shifted balance between litter inputs and heterotrophic respiration.

Given the changes in the ways in which forests have been used over the last century (8, 9), along with large changes in rates and directions of land-use change over the same time, the role of regrowth forest in the global carbon sink has recently received increased attention (2, 8–11). Large-scale estimates of the total carbon sink due to regrowth forest vary widely. Bookkeeping estimates have suggested a global regrowth forest uptake of 2.6 Pg C yr^{-1} over 2000-2009 (12) and of 1.2-1.64 Pg C yr^{-1} for the tropics during 1990-2010 (2, 13). In contrast, global vegetation models forced by land-use reconstructions have estimated a regrowth forest sink of 0.35-0.6 Pg C yr^{-1} for the 1990s (14) and 0.23-0.43 Pg C yr^{-1} for the 2000s (15). This uncertainty as to the size of the terrestrial carbon sink due to forest regrowth has profound consequences for our understanding of the global carbon cycle. Whereas the saturation point of a CO_2-induced sink remains highly

uncertain, a sink from forest regrowth is fundamentally bounded; once forests recovering from historical disturbance peaks have regained pseudo-equilibrium between carbon loss from disturbance and carbon gain from regrowth, or if carbon loss from disturbance begins to exceed carbon gain from regrowth, the net regrowth sink will disappear. Understanding the role of forest regrowth is thus a crucial step in assessing the extent to which we can continue to rely on the biosphere to mitigate rising atmospheric CO_2 concentrations. Further, understanding the geographic distribution of the sink allows actions to be taken to protect relevant ecosystems and maximize the magnitude of the carbon sink that can be realized in the future.

Here, we make use of the new Global Forest Age Database (GFAD), a global dataset of forest stand age derived from inventories and biomass data (16; Methods), to infer the recent sink of carbon in regrowth forest. We use this dataset to force a dynamic global vegetation model (DGVM) with explicit representation of demography in forest stand development (17) and to reproduce observed stand age for the year 2010. By individually tracking each newly established forest area, we are able to partition forest carbon fluxes between regrowth and old-growth stands. Further, using factorial simulations, one with fully-evolving environmental forcings (FF; climate, atmospheric CO_2 concentration, nitrogen deposition), and one in which those forcings are held constant at pre-industrial levels with only stand age structure being allowed to change (CF), we are able to discriminate the carbon sink resulting from changes in environmental forcing from that resulting from changes in forest demography. We focus on carbon fluxes of regrowth forest stands, and do not include carbon removed from the ecosystem in conjunction with forest clearing, except through legacy impacts upon the soil from the portion of litter left in the ecosystem.

We define old-growth forest as any forest stand more than 140 years old relative to our 2010 baseline. This definition represents a compromise between the 60-100 years reported for biomass recovery in individual forest stands (10, 18, 19), and the timescales of 140-400 years reported for recovery of pollen counts following large disturbance (20), indicative of the successional process. Succession is important because late successional trees typically live longer (21), reducing ecosystem-level carbon turnover rates. Our 140-year cut-off also coincides with the major shift in fuel sources from wood to fossil fuels during the industrial revolution, leading to reduced pressure on forest resources in many countries. Because the stand-age dataset is inferred based on existing forest properties, rather than historical land-use models as used in previous approaches, it allows calculation of the combined effect of all events that result in the establishment of a new forest stand, including forestry practices, land abandonment and natural disturbances such as fire.

Based on GFAD, we find a total old-growth forest area of 16.5 million km^2 in 2010, and 26.3 million km^2 of forest stands in a state of regrowth. Regrowth stands are concentrated in the northern extra-tropics, where the vast majority of stands fall into this category, whilst old-growth stands are concentrated in the tropical rainforest regions (Fig. 1). Mean total (i.e. across live biomass, litter and soil) carbon uptake over forested areas calculated by the LPJ-GUESS DGVM over 2001-2010 was 0.85 (0.66-0.96) Pg C yr^{-1} from old-growth stands and 1.30 (1.03-1.96) Pg C yr^{-1} from regrowth stands (Fig. 2). The ranges of our estimates reflect differences between sensitivity runs testing assumptions regarding the fate of disturbed material, the state of ecosystems before regrowth began and uncertainty in stand age (Methods). Of the regrowth sink, 0.53 (0.30-1.11 Pg C yr^{-1} would have occurred in the absence of any changes in environmental forcing over the 140 years prior to 2010, i.e. purely from the effects of changing forest demography on biomass, litter and soil carbon stocks. Across global regrowth forests, the enhancement in total carbon uptake rate due to demography is comparable to that due to environmental change (Fig.

2c, see SI Appendix, Fig. S2). Overall, the total forest sink increased from 1.74 (1.64-1.74) Pg C yr^{-1} over 1981-1990 to 2.15 (1.89-2.81) Pg C yr^{-1} over 2001-2010 (see SI Appendix, Fig. S2, Table S1, S2).

Our calculations are not directly comparable to those of the global carbon budget (1) in which any part of our uptake flux resulting from natural disturbance changes would be accounted for in the residual sink, with the remainder in the land-use change term. However, our mean environmental-change induced total uptake of 1.38 (1.36-1.43) Pg C yr^{-1} for forests over 1981-2010 is consistent with the total residual uptake across forest and non-forest ecosystems of 2.4±0.9 Pg C yr^{-1} over 1980-2009 given by Le Quéré et al. (1). Likewise the portion of this sink in the tropics and southern hemisphere forests (<23°N), 0.84 (0.82-0.87) Pg C yr^{-1}, compares favorably with the CO_2-induced sink across all landcovers in this region of 1.4±0.4 Pg C yr^{-1} over 1990-2007 estimated by Schimel et al. (7). Our total forest uptake is, however, around half that of Pan et al. (2), who estimated a total global forest sink of 4.05±0.67 Pg C yr^{-1} for 1991-2007, and our regrowth sink is only ca. 25% of that of Houghton et al. (12) - substantially smaller, even when allowance is made for our calculations being relative to a pre-industrial forest and those of Houghton et al. to a late 20th century forest. The Houghton et al. estimate includes regrowth following the mainly tropical practice of shifting cultivation, which would not be captured in our approach due to the comparatively coarse scale of the underlying data we have used, but as we show below, shifting-cultivation is unlikely to account for the disparity between our estimates. The magnitude of our age-forced regrowth sink is rather comparable to estimates by earlier studies forced by the HYDE land-use data (14, 15).

Our calculated old-growth sink is concentrated in tropical evergreen forests, whereas the regrowth sink is primarily located in the northern extratropics in deciduous broadleaf and evergreen needleleaf forests (Figs. 3a; see SI Appendix, Fig. S3, Tables S1, S2). Uncertainty in the tropical regrowth sink is large and results from large uncertainties in regrowth forest area (see SI Appendix, Fig. S4b) and from the dependence of soil carbon response on past land-use; post-agricultural soils (orange squares in Fig. 3) are already depleted in carbon and so lose less carbon during early re-establishment than forest soils do.

Area-adjusted total carbon uptake rate due to demography is highest in temperate broadleaf deciduous, needleleaf evergreen and mixed stands (see SI Appendix, Fig. S4c). This reflects both the intrinsic productivity of the forest types and the large fraction of older regrowth stands, for which accumulation of stem biomass dominates carbon balance. In contrast, young regrowth stands are more strongly affected by soil legacy emissions. Because most tropical broadleaf evergreen regrowth stands have been established within the last few decades, this results in a very low, or even net negative, overall carbon uptake rate due to demography for this forest type (see SI Appendix, Fig. S4). However, as the forest matures net carbon uptake rate increases, meaning that we can expect the regrowth carbon sink in tropical forests to intensify in the future, in the absence of further disturbance or adverse climate effects.

Our sink calculated for tropical regrowth forest, including environmental change, is an order of magnitude lower than that of Pan et al. (2). This discrepancy cannot be explained by differences in total forest area defined as regrowth, which was 30% of forest area between 23°S and 23°N in Pan et al. and is 48.1 (41.2-70.0) % based on the age-dataset we use in this study. Nor can uncertainties in initial soil state explain the discrepancy (see blue and orange squares in Figs. 2 and 3). The difference in sink estimates between our study and Pan et al.'s must therefore result either from differences in the locations or age of regrowth stands, or from differences in forest regrowth rates.

To explore the basis of the discrepancy in estimates of the carbon sink in forest regrowth, we also make simulations forcing our model with reconstructed time series of land-use from the latest version of the Land Use Harmonization project (LUH2; 22). This dataset was compiled to provide the land-use forcing for the upcoming 6th Coupled Model Intercomparison Project (CMIP6) and includes wood harvest and estimates of conversions from agriculture or pasture to forested land. LUH2 thus offers an independent, cross-check on the location and timing of the initialization of regrowth stands, and, all else being equal, should be expected to result in a smaller carbon sink in regrowth forest because natural disturbances are not included.

Global total carbon uptake in regrowth forest calculated using the LUH2 dataset is 0.78 Pg C yr^{-1} over 2001-2010, 49% of that calculated based on the GFAD dataset, of which 0.43 Pg C yr^{-1} (55%) would be realized in the absence of any environmental change since 1870 (Fig. 3b). The LUH2-forced simulations also yield a notable carbon uptake in extratropical regrowth stands, but much less than in simulations based on GFAD. The extent to which this deficit is due to natural disturbances, as opposed to differences in estimates of anthropogenic actions, cannot be deduced from our data. For tropical regrowth stands, LUH2 results in a 2.7× stronger sink than the standard GFAD simulation, despite LUH2 only defining 21.8% of the tropical forest as regrowth. We attribute the differences to two primary causes:
1) LUH2 does not account for the apparently relatively frequent natural disturbances and/or recent re-establishment occurring in the tropical forests. GFAD identifies a large area of very young tropical regrowth forest (see SI Appendix, Fig. S4b), consistent with Chazdon et al. (11), which is not yet old enough to be a net sink.
2) The GFAD dataset does not capture areas recovering from shifting cultivation or small-scale wood harvest. This is expected because it derives age classes in the dataset for tropical regions from a biomass product with a nominal resolution of 1 km^2 (23), too coarse to resolve the age distribution of local forest landscapes characterized by shifting cultivation practices. A recent assessment of the extent of shifting cultivation located much of it in tropical rainforest regions (24), and the results of that assessment are consistent with the locations of additional regrowth forest in central Africa and south-east Asia in the LUH2 dataset (see SI Appendix, Fig. S1). In addition, the 2000-2001 base year of the tropical biomass data (23) implies that the most recent changes in forest demography would not be included in GFAD.

Given the differing advantages of the GFAD and LUH2 datasets for the tropical region, we also calculated a combined estimate of regrowth forest carbon uptake for this region by adding the regrowth sink from transitions from reforestation in our LUH2 simulation to the regrowth sink calculated from the age dataset, for grid-cells which were identified as being subject to shifting cultivation (24; Methods). The risk of double-counting uptake here is limited because shifting cultivation is predominately located in the tropical broadleaf evergreen forest type, where demographic uptake is small in the age-forced simulations (Fig. 3a). The merged results (Fig. 3c; see SI Appendix, Tables S1, S2) raise our central estimate of the total tropical regrowth forest sink including environmental change from 0.12 to 0.27 Pg C yr^{-1} for 2001-2010, still well short of the 1.72 Pg C yr^{-1} for 2000-2007 reported by Pan et al. (2). We do not carry out any merging for the extratropics, as in these regions the locations and amounts of regrowth forest are much more consistent, and the age dataset makes use of an extensive network of ground-based surveys in these regions.

Overall, we simulate a small, but significantly (2 sample t-test at the 0.1% significance level, 23 844 grid-cells) greater enhancement of stand-scale woody growth rate as a result of environmental change in regrowth forest (median 40.3% enhancement relative to CF) than in old-growth forest (36.8%) for locations where both were simulated. The primary

reason for the woody growth enhancement appears to be a shift in forest composition towards pioneer species in regrowth forest, which grow more rapidly, and thus display a higher absolute growth enhancement as a result of environmental change. Experiments on seedlings and saplings have found that late-successional species often have a stronger relative response to elevated CO_2 than pioneer species (25), but this response is likely imposed on a lower absolute growth rate (21) and differences between mature trees are uncertain. It is also hypothesized that regrowth stands are subject to lower resource limitations than old growth stands and so better able to take advantage of CO_2 fertilization or growing season extension (26, 27). LPJ-GUESS is able to simulate differences in response due to changing light, water and N availability during different phases of regrowth, however the effect does not appear to be large in our simulations. Further constraints around the availability of limiting nutrients not considered here, including P and K (28), in regrowth forest stands are required to definitively assess this hypothesis.

Given that regrowth forest represents a large part of carbon uptake by current terrestrial ecosystems, how much further uptake can be expected if forest demography is allowed to reequilibrate? To assess this, we compare our FF simulation with an additional FF simulation over the same period in which the rate of forest disturbance (i.e. loss and reestablishment) averaged over the period 1981-2010 is repeated constantly throughout the simulation. This allows us to calculate the difference in carbon stocks relative to the carrying capacity under recent rates of disturbance. We exclude here the effects of any future environmental changes on the forest, or lagged effects of previous environmental changes, as comparison to a recent-historical baseline is less speculative. Tropical regrowth forest shows a much higher relative biomass deficit in 2010 than extratropical forests (Fig. 4a) because it is much younger, with a mean age of 18 (18-25) years as opposed to 52 (34-63) years in temperate deciduous forests and 72 (46-78) years in needleleaf evergreen forests. Remaining potential uptake due to demographic reequilibration in the biomass of current forests is, however, relatively equally distributed between tropical and extratropical regions (Fig. 4b), totaling 69 (44-131) Pg C, assuming that the disturbance regime of 1981-2010 is maintained. The same calculation based on CF simulations gives a remaining potential uptake of 60 (37-118) Pg C. Our FF estimate of 36 (26-70) Pg C for the entire tropical regrowth forest of 8.9 (7.6-13.1) Mkm^2 is consistent on a unit area basis with the 8.5 Pg C estimated by Chazdon et al. (11) for 2.4 Mkm^2 of regrowth forest in the Neotropics. Whether or not this uptake is realized will, of course, be sensitive to any future changes in disturbance regimes and the response of forests to environmental change.

By contrast, for soils and litter we find losses, rather than increases, in stocks, with a loss of 9 (8-17) Pg C relating to decomposition of litter following disturbances (see SI Appendix, Fig. S5). These changes are variable across forest types and for extratropical forests will likely take centuries to realize (29). Furthermore, they are sensitive to assumptions regarding the fate of disturbed material for which GFAD provides no information, and are likely to be affected if the previous land-use was not forest. As such, our confidence in the long-term soil carbon changes is low.

In addition to uncertainty in forest carbon uptake resulting from the datasets governing forest demography, our results might also be affected by the specific structure and parameterization of the model used. The LPJ-GUESS model has been favorably compared with inventory-based estimates of growth and stand structure from boreal, temperate and tropical forests, and simulated biomass and regrowth timescales are comparable to observations (see SI Appendix, Figs. S6, S7). Net primary production and net biome productivity lie in the middle of the range among current terrestrial biosphere models (30). To investigate the effects of different parameters and process assumptions encapsulated by other modelling systems we also cross-compare the LUH2 results from

LPJ-GUESS with those from two other DGVMs, LPJ and CABLE (Methods). As for LPJ-GUESS, the versions of both of these additional models used here also include explicit consideration of regrowth forest, tracking these stands through to maturity, but differ in the way they simulate internal stand dynamics (see SI Appendix). All models predict a similar pattern and magnitude of carbon sink in regrowth forest using the LUH2 dataset (Fig. 3b), with the only notable divergence being a stronger environmentally-induced carbon uptake in tropical regrowth forest by CABLE. This comparison thus reinforces our confidence in the magnitude of the regrowth fluxes inferred by our study, relative to the much larger carbon uptake suggested by some earlier studies.

We presented here a global assessment of the net carbon sink in current forests based on a new dataset of forest demography and on the latest global land-use change dataset, LUH2. The former is based on forest inventories and large-scale biomass data, the latter is based on HYDE (31), and thus ultimately on United Nations Food and Agriculture Organization statistics. Nevertheless, results based on both datasets are broadly consistent. The resulting estimates of total carbon uptake in regrowth forest are substantial, but lower than previous widely-cited estimates based on bookkeeping approaches (2, 12). Because regrowth forest is often found on land that was previously deforested, and because previous studies were based on similar observational data from forest plots, this may well imply that gross deforestation rates have previously been overestimated (2, 12). Forest degradation activities not considered here, such as selective harvest, edge-effects related to road building, and small fires, along with changes in background mortality rates (6), may also reduce the size of the intact or regrowth sink (32). Further work is required to assess whether such small-scale or partial disturbances further modify the demographic sink in global forests.

The persistence of an old-growth forest sink driven by environmental change hinges on the response of forests to elevated atmospheric CO_2 concentrations. Ultimately, the photosynthetic response to CO_2 saturates at concentrations well above current levels (33), but uptake in biomass may be substantially limited by nutrient availability at much lower CO_2 concentrations in many forests (34). In addition, there is some evidence that enhanced growth at elevated CO_2 may cause trees to proceed through their lifecycle faster, increasing biomass turnover rates and therefore limiting any CO_2-driven enhancements in the carbon sink (27). From a climate-change perspective, recent work also suggests that increases in growing season length due to climate change may also be limited by moisture availability (35), but CO_2-driven increases in water-use efficiency may compensate this (36). The point at which the environmental-change-driven sink will saturate thus remains highly uncertain. In contrast, much lower uncertainty surrounds the mechanism for sinks arising due to changes in forest demography. Such demographic sinks can be supported by practical management decisions – which indeed could also take into consideration important aspects of sustainability beyond carbon, such as biodiversity considerations (37). If current forest management practices continue, and the likelihood of tree mortality after controlling for forest demography remains constant, regrowth forest in both extratropical and tropical regions could continue to take up a large amount of carbon over the coming decades and contribute to climate change mitigation. But, ultimately, this substantial portion of the current terrestrial carbon sink is also transient in nature.

Methods

Forest age dataset. The Global Forest Age Dataset (GFAD) (16) is a forest stand age dataset developed as part of the EU FP7 project GEOCARBON and provides a distribution of stand age in 10-year age bins up to an age of 140 years from a base year of 2010 on a

0.5° grid. It draws on datasets of forest age distributions from forest inventories covering most temperate and boreal regions (Table S3). Forest age in tropical regions, where widespread inventories are not available, was estimated by applying climate-specific stand age-biomass curves (38) to a large-scale forest biomass dataset (23). With the biomass approach, an age-biomass curve was applied to the 1 km resolution biomass dataset (specific to one of three precipitation zones), and then the age classes were aggregated to the 10-year bins, and finally the area per age class was calculated as a fraction of the 0.5-degree grid cell. The tropical age-class distributions were assumed to be the same for the two tropical plant functional types, tropical evergreen and tropical raingreen. This approach has also recently been applied for the neo-tropics only as in Chazdon et al.(11). For downscaling the national or sub-national inventories to gridded forest distributions (using MODIS land cover), an assumption for homogeneous variance of age classes within each spatial domain was assumed. The MODIS Collection 5.1 land cover dataset was first aggregated from 500 m land cover classes to 0.5° forest type fractions (needleleaf evergreen, broadleaf evergreen, needleleaf deciduous, broadleaf deciduous) following the approach of Poulter et al.(39) and then used for downscaling. The gridded age class distribution dataset thus matches the forest inventory at the same administrative scales, and the reliability of the spatial downscaling approach has been compared with forest canopy height maps (40), as a proxy for age, showing the expected relationship between older forests and taller forest canopies across all major forest types (see SI Appendix, Fig. S8). Calculation of confidence intervals for GFAD is described in the SI Appendix.

Modelling forced by GFAD. LPJ-GUESS explicitly represents the influence of disturbances on forest structure across the landscape using a gap model approach on multiple forest patches (here 50) (17). Following a stand-clearing disturbance event regrowth occurs following secondary succession. Forest structure within patches is modelled using age cohorts, allowing competition for light, water and nitrogen by plants of different type and sizes (41). Soil carbon and nitrogen cycling is based on the CENTURY model (42). LPJ-GUESS was initialized with a 1570 year spin-up to 1870 using repeated, detrended 1901-1910 climate from the CRU-NCEP dataset (43). The effect on our results of using 10-year vs 30-year climate periods when averaged over a 30-year period (i.e. 1981-2010) was negligible. Atmospheric CO_2 mixing ratio was fixed at 286 ppm during spin-up and atmospheric nitrogen deposition at the 1860-1869 values from Lamarque et al. (44). Stand-clearing disturbances during spin-up were applied randomly according to a typical return period, which was here specified at grid cell level based on GFAD, as described in the SI Appendix.

Following the initialization of primary forest during spin-up, from 1870 onwards forest loss was prescribed each year in order to recreate the 2010 stand age structure and composition in GFAD. These forest losses were treated as a land-use transition, creating a new patch representing that area of newly-established forest upon which regrowth was explicitly tracked. We thus created up to 140 new patches per grid cell and GFAD forest type over the course of the simulation. Forest loss at transitions was treated as harvest, with 66% of the harvested material being removed from the ecosystem. The standard random disturbance parameterization used during spin-up was turned off in these new patches, but continued in the primary forest because GFAD only captures the date of the most recent disturbance (there may have been multiple disturbances in any one location since 1870). Because only areas with random background disturbance intervals typically much longer than 140 years (median 438 years) remain as primary forest in the period 1981-2010, this provides only a minimal inconsistency during the period for which we analyze primary forest fluxes. We designate this primary forest as "old-growth" during our analyses for the period 1981-2010. The analysis herein concentrates on the fluxes within forested ecosystems since the point of reestablishment, we have thus not directly

addressed the size of fluxes resulting from products removed from the ecosystem, or from fires, primarily because GFAD does not allow us to assign a time for forest loss events. Simulations were conducted with the best estimate and the 5% and 95% confidence limits of the GFAD stand age. To calculate the sink in regrowth forest less than 50 years old, these simulations were repeated with only stands initialized between 1960 and 2010 being assigned to regrowth forest.

Full forcing (FF) simulations used transient CRU-NCEP climate (from 1901 onwards) and atmospheric CO_2 mixing ratios as used for the global carbon project (43), and atmospheric N deposition (44) for the period 1870-2010. Constant forcing (CF) simulations continued with spin-up forcing throughout. All simulations were carried out at 0.5° resolution.

To characterize uncertainties due to data limitations, the following sensitivity simulations were performed with FF and CF setups.

S1) GFAD gives no information on disturbance type. In S1 simulations disturbed material remained in the ecosystem in grid cells defined as wild forest by Ellis et al. (45), rather than being partially removed.

S2) GFAD gives no information on previous land-use. In S2 all land except wild forest was initialized as cropland, providing the most extreme departure from old-growth forest used in the standard simulations.

S3) To test the influence of the disturbance return period used during spin-up, an additional sensitivity increased this return period by 50%.

More details on S1 and S2 are given in the SI Appendix.

The potential remaining uptake due to forest regrowth was characterized by comparing the carbon density in the GFAD-forced simulations with that in a simulation in which only old-growth forest was simulated at that location, both for FF and CF forcings. These calculations were carried out for standard and S1 set-ups. Relative carbon density change ΔC_{rel} (%) was calculated as $((C_{reg}/C_{OG}) - 1) \times 100$, where C_{reg} and C_{OG} are the carbon densities (kg C m^{-2}) for that forest type and ecosystem compartment (i.e. live biomass or soil/litter) in regrowth and old-growth forest respectively. The mean ΔC_{rel} across the area of the forest type was then calculated. Total missing biomass carbon was calculated as $(C_{OG} - C_{reg}) \times A_R$, where A_R is the regrowth forest area in the grid cell in m^2, and then summed over the area of the forest type.

Modelling forced by LUH2. LUH2-forced simulations for LPJ-GUESS, LPJ (46) and CABLE (47) DGVMs were carried out using a common protocol applying the same atmospheric forcing data as for the GFAD-forced simulations described above for both FF and CF settings. Spin-up followed model-specific conventions, with LPJ-GUESS using environmental forcing as described above. Transitions to regrowth forest were prescribed following the secondary land classification (including secondary land created by wood harvest) in LUH2. LPJ-GUESS simulations were initialized in 1700, LPJ in 1860 and CABLE in 1590. For LPJ-GUESS and LPJ, only transitions after 1870 were classified as regrowth forest for the purposes of this analysis. More information on setup of the DGVMs is given in the SI Appendix. Combined GFAD and LUH2 uptake (Fig. 3c) was calculated by adding uptake from stands which had transitioned to forest land-use in LUH2-forced simulations to that from GFAD-forced simulations in grid cells where shifting cultivation had low, moderate or height occurrence according to Heinimann et al. (24).

Area masking. Our results are restricted to current forest area. This was defined based on ESA CCI landcover (48), with all forest landcover types with at least 15% canopy cover being included (codes: 50, 60, 61, 62, 70, 71, 72, 80, 81, 82, 90, 100, 160 and 170). The landcover at a nominal 300 m resolution was aggregated to give fractional coverage of forest at 0.5° resolution (see SI Appendix, Dataset S1). To ensure consistency, all model

outputs were rescaled according to this ESA CCI forest cover fraction when calculating global and regional totals. Relative forest cover fractions from the GFAD and LUH2 datasets were used to break down the forest area into old-growth and regrowth in each grid cell. Classification of forest types also followed ESA CCI, with the mapping used in this analysis shown in the SI Appendix, Table S4. A map of these forest types is shown in the SI Appendix, Fig. S9, along with the data in Dataset S2.

Data availability. Data from the model simulations underlying this paper can be obtained from the corresponding author on request. Source code for the LPJ-GUESS, LPJ and CABLE models is available on request from the developers. Forest mask files are included in the SI Appendix.

Acknowledgements

TP and AA acknowledge support from EU FP7 grant LUC4C (grant no. 603542), and the Helmholtz Association in its ATMO programme. TP also acknowledges support from the European Research Council (ERC) under the EU Horizon 2020 programme (grant no. 758873, TreeMort). LC acknowledges support from a National Aeronautics and Space Administration Earth and Space Science Fellowship (2016-2019). VH acknowledges support from the Earth Systems and Climate Change Hub, funded by the Australian Government's National Environmental Science Program. ML acknowledges funding through the SUMFOREST ERA-NET project FOREXCLIM. This study contributes to the Strategic Research Areas BECC and MERGE. This is paper number 33 of the Birmingham Institute of Forest Research. The authors thank Louise Chini, Andreas Heinimann, Peter Anthoni, Christopher Woodall and Mart-Jan Schelhaas for advice and data provision.

References

1. Quéré C Le, et al. (2018) Global Carbon Budget 2017. *Earth Syst Sci Data* 10:405–448.
2. Pan Y, et al. (2011) A large and persistent carbon sink in the world's forests. *Science* 333(2011):988–993.
3. Odum EP (1969) The Strategy of Ecosystem Development. *Science* 164(3877):262–270.
4. Sousa WP (1984) The role of disturbance in natural communities. *Annu Rev Ecol Syst* 15:353–391.
5. Luyssaert S, et al. (2008) Old-growth forests as global carbon sinks. *Nature* 455(September):213–215.
6. Brienen RJW, et al. (2015) Long-term decline of the Amazon carbon sink. *Nature* 519(7543):344–348.
7. Schimel D, Stephens BB, Fisher JB (2015) Effect of increasing CO_2 on the terrestrial carbon cycle. *Proc Natl Acad Sci U S A* 112(3):436–441.
8. Erb K-H, et al. (2013) Bias in the attribution of forest carbon sinks. *Nat Clim Chang* 3(10):854–856.
9. Naudts K, et al. (2016) Europe's forest management did not mitigate climate warming. *Science* 351(6273):597–600.
10. Poorter L, et al. (2016) Biomass resilience of Neotropical secondary forests. *Nature* 530(7589):211–214.
11. Chazdon RL, et al. (2016) Carbon sequestration potential of second-growth forest regeneration in the Latin American tropics. *Sci Adv* 2:e1501639.
12. Houghton RA, et al. (2012) Carbon emissions from land use and land-cover change. *Biogeosciences* 9(12):5125–5142.
13. Houghton RA (2013) The emissions of carbon from deforestation and

degradation in the tropics: past trends and future potential. *Carbon Manag* 4(5):539–546.
14. Shevliakova E, et al. (2009) Carbon cycling under 300 years of land use change: Importance of the secondary vegetation sink. *Global Biogeochem Cycles* 23(2):GB2022.
15. Kondo M, et al. (2018) Plant regrowth as a driver of recent enhancement of terrestrial CO_2 uptake. *Geophys Res Lett* 45(10):4820–4830.
16. Poulter B, et al. (2018) *The global forest age dataset (GFADv1.0), link to NetCDF file* Available at: https://doi.pangaea.de/10.1594/PANGAEA.889943.
17. Smith B, et al. (2014) Implications of incorporating N cycling and N limitations on primary production in an individual-based dynamic vegetation model. *Biogeosciences* 11(7):2027–2054.
18. Teobaldelli M, Somogyi Z, Migliavacca M, Usoltsev VA (2009) Forest Ecology and Management Generalized functions of biomass expansion factors for conifers and broadleaved by stand age, growing stock and site index. *For Ecol Manage* 257:1004–1013.
19. Martin PA, Newton AC, Bullock JM (2013) Carbon pools recover more quickly than plant biodiversity in tropical secondary forests. *Proc R Soc B Biol Sci* 280:20132236.
20. Cole LES, Bhagwat SA, Willis KJ (2014) Recovery and resilience of tropical forests after disturbance. *Nat Commun* 5(May):1–7.
21. Huston M, Smith T (1987) Plant Succession: Life History and Competition. *Am Nat* 130(2):168–198.
22. Hurtt G, Chini L, Sahajpal R, Frolking S (2017) Harmonization of global land-use change and management for the period 850-2100. Available at: http://luh.umd.edu/data.shtml [Accessed December 15, 2017].
23. Saatchi SS, et al. (2011) Benchmark map of forest carbon stocks in tropical regions across three continents. *Proc Natl Acad Sci* 108:9899–9904.
24. Heinimann A, et al. (2017) A global view of shifting cultivation: Recent, current, and future extent. *PLoS One* 12(9):e0184479.
25. Kerstiens G (2001) Meta-analysis of the interaction between shade-tolerance, light environment and growth response of woody species to elevated CO_2. *Acta Oecologica* 22:61–69.
26. Körner C (2006) Plant CO_2 responses: an issue of definition, time and resource supply. *New Phytol* 172:393–411.
27. Körner C (2017) A matter of tree longevity. *Science* 355(6321):130–131.
28. Baribault TW, Kobe RK, Finley AO (2017) Tropical tree growth is correlated with soil phosphorus, potassium, and calcium, though not for legumes. *Ecol Monogr* 82(2):189–203.
29. Pugh TAM, et al. (2015) Simulated carbon emissions from land-use change are substantially enhanced by accounting for agricultural management. *Environ Res Lett* 10(12). doi:10.1088/1748-9326/10/12/124008.
30. Sitch S, et al. (2015) Recent trends and drivers of regional sources and sinks of carbon dioxide. *Biogeosciences* 12(3):653–679.
31. Goldewijk KK, Beusen A, Doelman J, Stehfest E (2017) Anthropogenic land use estimates for the Holocene - HYDE 3.2. *Earth Syst Sci Data* 9(2):927–953.
32. Baccini A, et al. (2017) Tropical forests are a net carbon source based on aboveground measurements of gain and loss. *Science* 358(6360):230–234.
33. Ainsworth EA, Rogers A (2007) The response of photosynthesis and stomatal conductance to rising [CO_2]: mechanisms and environmental interactions. *Plant, Cell Environ* 30:258–270.
34. Wieder WR, Cleveland CC, Smith WK, Todd-brown K (2015) Future productivity and carbon storage limited by terrestrial nutrient availability. *Nat Geosci* 8:441–444.

35. Buermann W, et al. (2018) Widespread seasonal compensation effects of spring warming on northern plant productivity. *Nature* 562:110–115.
36. Ahlström A, et al. (2015) The dominant role of semi-arid ecosystems in the trend and variability of the land CO_2 sink. *Science* 6237:895–899.
37. Strassburg BBN, et al. (2010) Global congruence of carbon storage and biodiversity in terrestrial ecosystems. *Conserv Lett* 3(2):98–105.
38. Marin-Spiotta E, Cusack DF, Ostertag R, Silver WL (2008) Trends in above and belowground carbon with forest regrowth after agricultural abandonment in the neotropics. *Post-Agricultural Succession in the Neotropics*, ed Myster RW (Springer).
39. Poulter B, et al. (2011) Plant functional type mapping for earth system models. *Geosci Model Dev* 4:993–1010.
40. Simard M, Pinto N, Fisher JB, Baccini A (2011) Mapping forest canopy height globally with spaceborne lidar. *J Geophys Res* 116:G04021.
41. Smith B, Prentice IC, Sykes MT (2001) Representation of vegetation dynamics in modelling of European ecosystems: comparison of two contrasting approaches. *Glob Ecol Biogeogr* 10:621–637.
42. Parton WJ, et al. (1993) Observations and modeling of biomass and soil organic matter dynamics for the grassland biome worldwide. *Global Biogeochem Cycles* 7(4):785–809.
43. Le Quéré C, et al. (2016) Global Carbon Budget 2016. *Earth Syst Sci Data* 8:605–649.
44. Lamarque JF, et al. (2013) Multi-model mean nitrogen and sulfur deposition from the atmospheric chemistry and climate model intercomparison project (ACCMIP): Evaluation of historical and projected future changes. *Atmos Chem Phys* 13(16):7997–8018.
45. Ellis EC, Goldewijk KK, Siebert S, Lightman D, Ramankutty N (2010) Anthropogenic transformation of the biomes, 1700 to 2000. *Glob Ecol Biogeogr* 19(5):589–606.
46. Sitch S, et al. (2003) Evaluation of ecosystem dynamics, plant geography and terrestrial carbon cycling in the LPJ dynamic global vegetation model. *Glob Chang Biol* 9(2):161–185.
47. Haverd V, Smith B, Nieradzik LP, Briggs PR (2014) A stand-alone tree demography and landscape structure module for Earth system models: Integration with inventory data from temperate and boreal forests. *Biogeosciences* 11:4039–4055.
48. ESA (2017) ESA CCI Land Cover dataset (v 1.6.1). Available at: https://www.esa-landcover-cci.org/?q=node/169 [Accessed June 29, 2017].

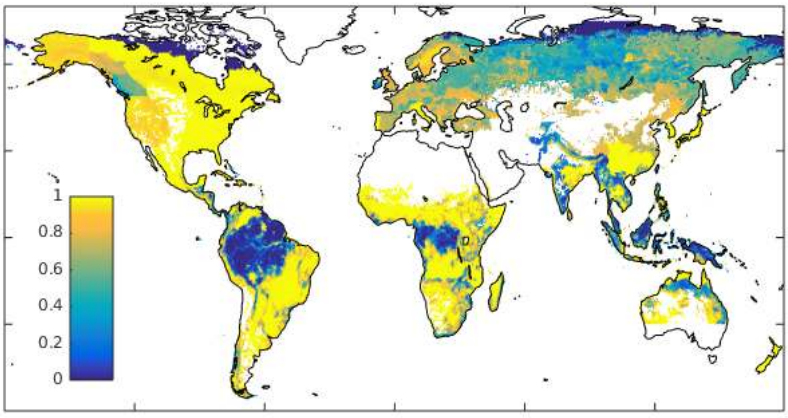

Figure 1. Fraction of forest defined as regrowth (less than 140 years old) in the age dataset for the year 2010. The blank area in southern Australia occurs because no data for this area exists in the GFAD dataset.

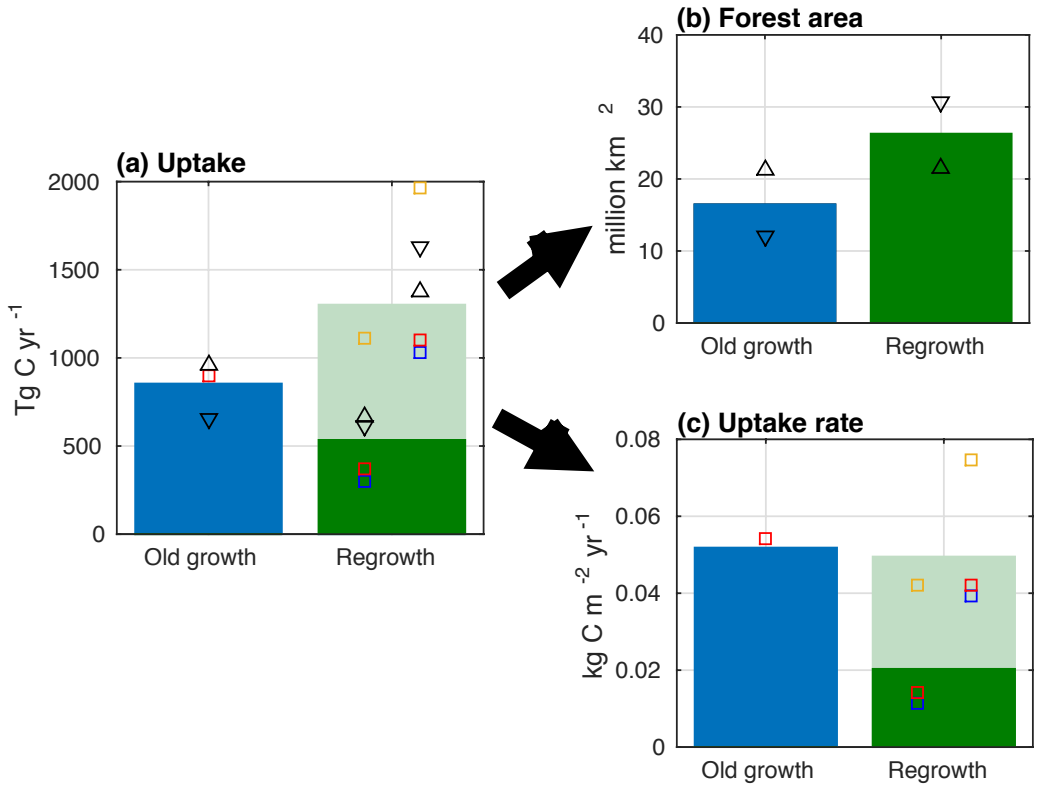

Figure 2. 2001-2010 mean carbon sink in global forests partitioned between old-growth and regrowth forests, as calculated by LPJ-GUESS forced by GFAD. (a) Total uptake in old-growth and regrowth forest. Dark green shows the fraction of the regrowth sink that would have occurred in the absence of any environmental change since 1870 (CF), whilst the light green bar shows the additional flux including all environmental forcing (FF). (b) Total forest area in old growth and regrowth categories. (c) Uptake rate per area. Results from sensitivity studies are illustrated with additional symbols. The blue square shows the sensitivity to assumptions about the fate of cleared material (Methods, S1), the orange square to assumptions about land-use type prior to forest regrowth (S2) and the red square to the assumed rate of disturbance in spin-up (S3). The downwards pointing arrow is forced by the 5% confidence limit of the stand age distribution and the upwards pointing arrow the 95% confidence limit. For regrowth forest these sensitivity simulations are shown both for CF (left of regrowth bar) and FF (right of regrowth bar). By definition, the sink in old-growth forest is only driven by changes in environmental forcing (FF) and hence has no CF component.

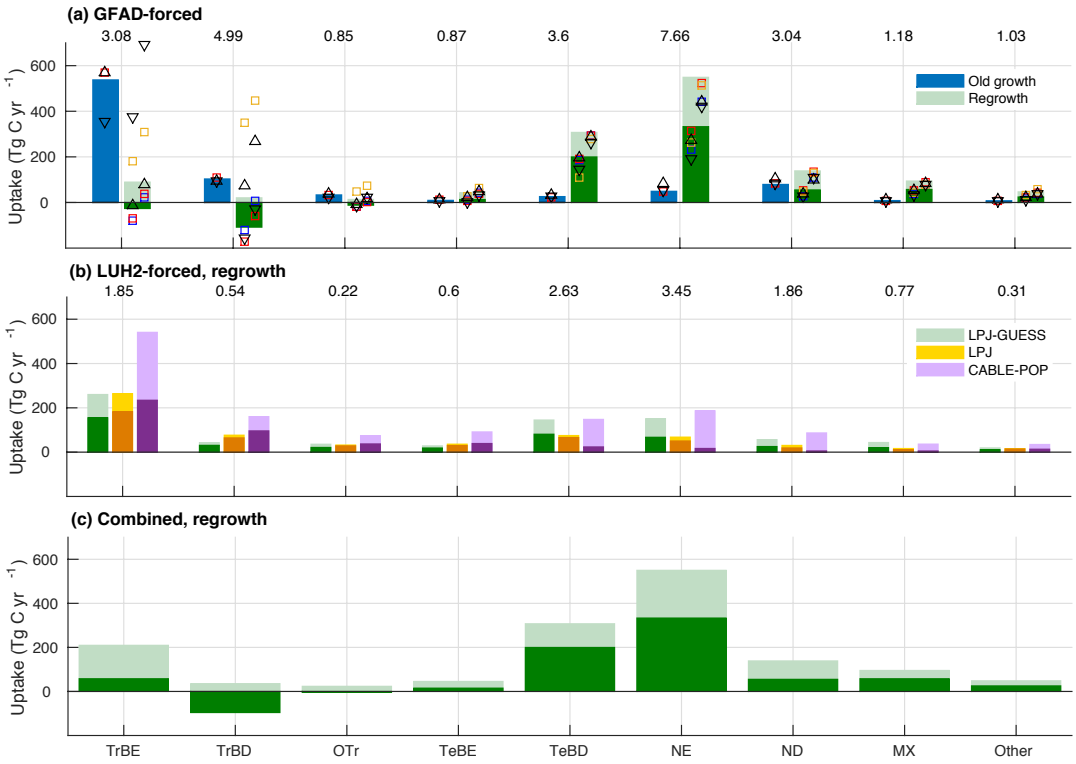

Figure 3. (a) 2001-2010 mean carbon sink in global forests partitioned between old-growth and regrowth forests, as calculated by LPJ-GUESS forced by GFAD. The sink is split by forest type (for forest type distribution see SI Appendix, Fig. S4). Coloring and symbols as for Fig. 2. (b) 2001-2010 mean carbon sink in regrowth forests, forced by the LUH2 land-use dataset, as calculated for three different DGVMs. More intense colors show the sink in CF simulations, and lighter shades additional sink due to environmental change (FF). Numbers above the bars in panels a and b show the total regrowth forest area in each classification in units of million km^2. (c) Regrowth forest sink as estimated from combining the GFAD and LUH2 datasets best estimates (see main text), coloring as for panel a. Forest types are: tropical broadleaved evergreen (TrBE), tropical broadleaved deciduous (TrBD), other tropical forest (OTR), temperate broadleaved evergreen (TeBE), temperate broadleaved deciduous (TeBD), needleleaved evergreen (NE), needleleaved deciduous (ND), broadleaved-needleleaved mixed forest (MX), other forest (Other). Forest type classification was based on ESA CCI landcover (see Methods).

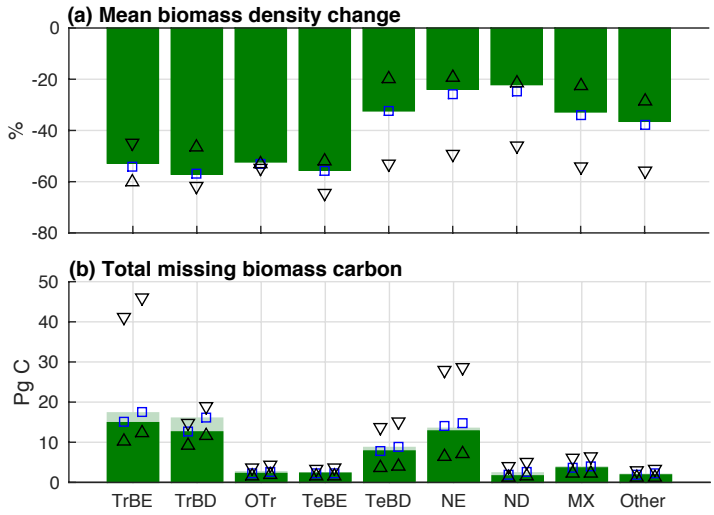

Figure 4. (a) Percentage difference between biomass in regrowth forest (2010 values) and the biomass that would exist at that location if the forest was in equilibrium with the mean 1981-2010 forest disturbance rate, averaged over each forest type and based on LPJ-GUESS simulations forced by GFAD. (b) Total missing biomass carbon for each forest type, found by differencing the carbon densities of old-growth and regrowth stands in 2010 and multiplying by regrowth area, based on the CF simulation (dark green) and the FF simulation (light green). The symbols show sensitivity simulations, as in Fig. 2. Difference between CF and FF in panel **a** was minimal, and thus only CF is shown.

Supporting Information Appendix for:

The role of forest regrowth in global carbon sink dynamics

Contains

- Supporting Methods
- Supporting Tables S1 to S4
- Supporting Figures S1 to S9
- Supporting Datasets S1 and S2
- Supporting References

Supporting Methods

Confidence intervals on GFAD. We created two additional age map estimates building on the standard version of GFAD (1), representing the lower and upper confidence intervals of forest stand age distribution. In the regions where the stand age distribution was calculated based on forest inventories we applied an age uncertainty of ±40% based on error in age determination reported by the US Forest Service (2). These age uncertainties are reported as a 90% confidence interval, but applying a best fit curve to their age versus uncertainty data finds 95% confidence interval to be almost identical. The estimate of ±40% likely errs on the large side because of error cancellation when aggregated over space. We estimated uncertainty in the tropical regions by propagating the 95% confidence intervals in biomass (3) through the biomass ages curves.

Disturbance during LPJ-GUESS spin-up in GFAD-forced simulations. We calculated a stand-replacing-disturbance return period based on the rate of forest loss in the period 1981-2010 of the GFAD dataset. This was carried out by dividing the total fraction of forest established in each 0.5° grid cell over 1981-2010 by 30 years in order to give a mean annualized forest establishment rate. It was assumed that disturbance rates and establishment rates were equivalent. This mean rate was then converted into a disturbance rotation period by dividing the total forest area fraction in a grid-cell in 2010 by the annual disturbance rate in that grid-cell. We assume that this mean disturbance rotation period per grid-cell is equivalent to the return period at any point within that grid-cell. Return periods were capped at 1000 years and for grid cells with very low forest area or no data, a period of 100 years was assumed. We acknowledge that this assumes current disturbance rates, including forest harvest, are applied in the pre-industrial period, but given that very limited data exists on disturbance rates across biomes, this choice is a substantial improvement over considering a single universal value. The assumption will be particularly valid in the tropical forest, where stand-replacing disturbances are rare events (4, 5). Disturbance events during spin-up were partitioned between fire and "other" disturbances using the LPJ-GUESS fire model (6). For "other" disturbances the disturbed biomass was transferred to litter.

Sensitivity simulations. Additional information on sensitivity set-ups S1 and S2 is as follows:

S4) There is uncertainty regarding the fate of disturbed material, because GFAD gives no information about the type of forest disturbance. In the standard simulation it is assumed that 66% of disturbed material on the remaining land is removed from the ecosystem through harvest or burning. As not all natural disturbances result in wood being removed or burnt, sensitivity simulations were also conducted where this disturbed material remained in the ecosystem. However, as it would be unrealistic to assume that all disturbed material remains in the ecosystem in most forests where humans are active, this sensitivity test was only applied in grid cells defined as wild forest by Ellis et al. (7) (after aggregating to 0.5° from 5 arc minute resolution based on the mode classification).

S5) GFAD gives no information on previous land-use, which may be managed forest, pasture or cropland, rather than the old-growth forest assumed in our standard simulations. The implications of this may be particularly large for soil carbon stocks (8). As croplands provide the most extreme differences in soil carbon compared to forest soils (9, 10), we tested the sensitivity to this assumption by carrying out a simulation where all land was initialized as cropland. Crop type and fertilization rate were prescribed as in Olin et al. (48), extrapolating these following the nearest neighbor rule for grid-cells in which no cropland was simulated in that study. Because this sensitivity test would be totally unrealistic in a wild forest, grid-cells defined as wild forest by Ellis et al. (7) were simulated using standard settings.

Modelling forced by LUH2. The version of LPJ used here was an update of Sitch et al. (12) which allows to explicitly track fractions of regrowth forest within each grid cell (10-year stand age-classes from 1-100 {1-10 years, 11-20 years, ... , 91-100 years}, 101-150 years, and 150+ years; corresponding to stand age-classes typical of forest inventory data). Among stand age-classes in a grid cell, climate, atmospheric CO_2 concentration and soil texture are similar, whereas resources for plants (e.g., space, light, water) may differ depending on demand; as such, processes related to photosynthesis, plant competition and heterotrophic respiration are simulated at the level of the age-class. Stand age-classes are created via fire on stands with no history of land-use change, whereas on forest stands with a history of land use change, age-classes are created by fire and via land-use transitions.

LPJ does not model size cohorts within stand age classes, but follows an area-based approach to within-stand dynamics (12). Competitive advantages occur when a plant functional type (PFT) has greater growth efficiency, more positive annual carbon balance, and greater tolerances to heat stress and water availability. Less competitive PFTs undergo reductions in PFT-specific tree densities (i.e. mortality). Explicit competition for light occurs if the total tree foliar projective cover is above 95% of the stand area. In which case, shading mortality is partitioned among PFTs according to the annual allocation to leaf area to maintain a maximum tree foliar projective cover in the stand of 95%.

In LPJ, deforestation results in 100% of heartwood biomass and 50% of sapwood biomass being removed from the ecosystem, with the remaining biomass being transferred to litter pools. Harvest results in 60% of heartwood and sapwood being removed from the ecosystem.

The version of the CABLE model used here incorporates the POP vegetation demographic model which is fully described in Haverd et al. (13, 14). Competition between cohorts in CABLE is governed by self-thinning, as influenced by crowding of crowns, and size-dependent resource limitation constraints (14). CABLE used coefficients for removal of harvested and cleared biomass from the ecosystem following (15).

All three DGVMs simulated transitions due to both forest harvest and land abandonment in the LUH2-forced simulations. LPJ-GUESS tracked these two transition types separately.

Supporting Tables

Table S1. Decadal regrowth forest areas and carbon uptake calculations for regrowth forest under constant forcing.

	TrBE	TrBD	OTr	TeBE	TeBD	NE	ND	MX	Other	Units
1981-1990										
Regrowth area, GFAD	0.88	0.56	0.19	0.37	2.60	6.37	2.39	0.85	0.66	M km^2
Regrowth area, LUH2	1.48	0.47	0.20	0.49	2.49	3.12	1.62	0.70	0.28	
GFAD, LPJ-GUESS[1]	59 (23 – 359)	13 (6 – 35)	7 (3 – 9)	6 (-2 – 10)	130 (31 – 152)	238 (44 – 238)	39 (12 – 39)	44 (3 – 45)	20 (3 – 20)	Tg C yr^{-1}
LUH2, LPJ-GUESS	115	32	17	14	73	50	16	17	9	
Combined, LPJ-GUESS[2]	135	27	14	10	130	239	39	45	23	
LUH2, LPJ	149	54	23	15	56	39	19	12	12	
LUH2, CABLE	173	61	26	16	23	4	5	5	12	
1991-2000										
Regrowth area, GFAD	1.26	0.98	0.28	0.55	2.96	6.87	2.80	0.92	0.76	M km^2
Regrowth area, LUH2	1.66	0.5	0.21	0.54	2.56	3.30	1.72	0.74	0.30	
GFAD, LPJ-GUESS[1]	70 (23 – 450)	18 (3– 62)	8 (3 – 14)	8 (0 – 17)	161 (80 – 169)	276 (112 – 276)	33 (8 – 33)	50 (20 – 50)	22 (10 – 22)	Tg C yr^{-1}
LUH2, LPJ-GUESS	130	31	20	17	78	59	21	19	10	
Combined, LPJ-GUESS[2]	147	31	16	11	161	278	33	51	25	
LUH2, LPJ	139	57	23	17	42	35	16	9	12	
LUH2, CABLE	176	73	31	32	29	19	1	4	15	
2001-2010										
Regrowth area, GFAD	3.08	4.99	0.85	0.87	3.60	7.66	3.04	1.18	1.03	M km^2
Regrowth area, LUH2	1.85	0.54	0.22	0.60	2.63	3.45	1.86	0.77	0.31	
GFAD, LPJ-GUESS[1]	-27 (-80 – 375)	-108 (-169 – 347)	-12 (-21 – 50)	13 (0 – 29)	200 (111 – 200)	333 (191 – 333)	55 (29 – 55)	57 (34 – 57)	24 (13 – 34)	Tg C yr^{-1}
LUH2, LPJ-GUESS	155	31	21	19	81	67	25	20	11	
Combined, LPJ-GUESS[2]	58	-96	-4	15	200	333	55	58	25	
LUH2, LPJ	182	64	28	30	66	50	19	11	14	
LUH2, CABLE	234	96	37	39	24	17	6	5	13	

[1] Figures in parentheses are ranges across all sensitivity simulations.
[2] Combined results forced by GFAD and LUH2, as in Fig. 3c.

Table S2. Decadal regrowth forest areas carbon uptake calculations for regrowth forest under full forcing.

	TrBE	TrBD	OTr	TeBE	TeBD	NE	ND	MX	Other	Units
1981-1990										
Regrowth area, GFAD	0.88	0.57	0.19	0.37	2.60	6.37	2.29	0.85	0.66	M km^2
Regrowth area, LUH2	1.48	0.47	0.20	0.49	2.49	3.12	1.62	0.70	0.28	
GFAD, LPJ-GUESS[1]	96 (44 – 542)	26 (14 – 44)	12 (6 – 15)	19 (5 – 23)	209 (90 – 227)	362 150 – 362)	77 (35 – 77)	72 (28 – 72)	11 (14 – 32)	Tg C yr^{-1}
LUH2, LPJ-GUESS	176	40	25	23	128	107	40	33	15	
Combined, LPJ-GUESS[2]	197	42	21	24	209	364	77	73	34	
LUH2, LPJ	188	61	27	27	66	64	29	14	15	
LUH2, CABLE	360	94	51	59	108	133	48	26	31	
1991-2000										
Regrowth area, GFAD	1.26	0.98	0.28	0.55	2.96	6.87	2.80	0.92	0.76	M km^2
Regrowth area, LUH2	1.66	0.5	0.21	0.54	2.56	3.30	1.72	0.74	0.30	
GFAD, LPJ-GUESS[1]	126 (62 – 687)	52 (30 – 87)	19 (9 – 26)	27 (18 – 37)	255 (173 – 258)	432 (268-432)	75 (46 – 75)	76 (50 – 76)	37 (24 – 38)	Tg C yr^{-1}
LUH2, LPJ-GUESS	215	44	31	29	136	129	42	35	17	
Combined, LPJ-GUESS[2]	238	67	29	31	255	434	75	77	40	
LUH2, LPJ	212	69	29	34	69	64	25	13	17	
LUH2, CABLE	417	121	60	76	137	160	65	32	34	
2001-2010										
Regrowth area, GFAD	3.08	4.99	0.85	0.87	3.60	7.66	3.04	1.18	1.03	M km^2
Regrowth area, LUH2	1.85	0.54	0.22	0.60	2.63	3.45	1.86	0.77	0.31	
GFAD, LPJ-GUESS[1]	89 (21 – 692)	21 (-61 – 449)	13 (2 – 75)	43 (33 – 64)	307 (265 – 307)	549 (420 – 549)	139 (101 – 139)	94 (76 – 94)	47 (38 – 60)	Tg C yr^{-1}
LUH2, LPJ-GUESS	260	43	36	28	145	150	57	44	19	
Combined, LPJ-GUESS[2]	210	35	23	45	307	550	139	95	48	
LUH2, LPJ	264	77	32	36	75	68	30	16	16	
LUH2, CABLE	541	160	74	91	148	187	87	36	35	

[1] Figures in parentheses are ranges across all sensitivity simulations.
[2] Combined results forced by GFAD and LUH2, as in Fig. 3c.

Table S3. Source of information underlying GFAD.

Country	Source	Time Period
United States	US Forest Inventory and Analysis (v5.1) (state summaries)	2000s
Russia	IIASA Russian Forests and Forestry Database	2000s (late)
Canada	Canadian Forest Inventory (state summaries)	2000-2006
Europe	EFISCEN (32 countries)	2000s
China	6th National Forest Inventory	1999-2003
Kazakhstan	National Forest Inventory	2000s
New Zealand	National Forest Inventory	2000s
Mongolia	National Forest Inventory	2000s
Japan	2005 National Forest Inventory	2005
Pan tropics	Saatchi et al. (3)	2000s

Table S4. Mapping of ESA landcover classes to forest types used in this analysis.

Code	Forest class	ESA landcover classes	Additional conditions
TrBE	Tropical broadleaved evergreen	50	latitude ≤ 23°
TrBD	Tropical broadleaved deciduous	60, 61, 62	latitude ≤ 23°
OTr	Other tropical forest	100, 160, 170	latitude ≤ 23°
TeBE	Temperate broadleaved evergreen	50	latitude > 23°
TeBD	Temperate broadleaved deciduous	60, 61, 62	latitude > 23°
NE	Needleleaved evergreen	70, 71, 72	n/a
ND	Needleleaved deciduous	80, 81, 82	n/a
MX	Broadleaved-needleleaved mixed forest	90	n/a
Other	Other forest	100, 160, 170	latitude > 23°

Supporting Figures

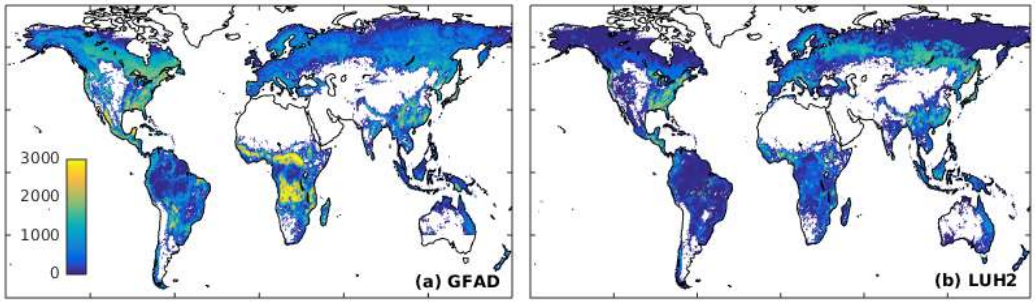

Figure S1. Regrowth forest area (km^2) per 0.5° grid cell based on GFAD (a) and LUH2 (b). Note that the total forest area is constrained by ESA CCI forest cover (see Methods). All cells containing at least 1% forest cover are shown here.

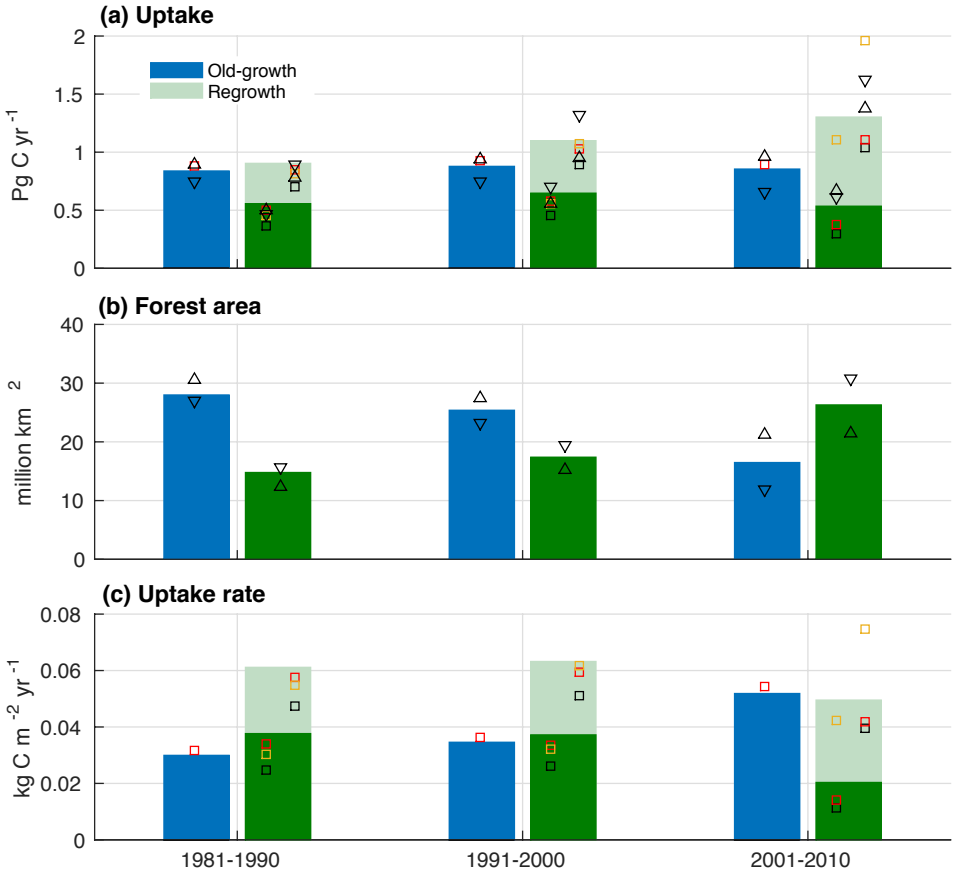

Figure S2. Total carbon uptake (a), forest area (b) and uptake rate (c), split by old-growth and regrowth forest for the three decades preceding 2010. Sensitivity studies are shown as for Fig. 2. Note that the primary forest area in 1981-1990 and 1991-2000 may be slightly overestimated because the base time period for the stand age data is 2001-2010 and we have no information for the age of stands in e.g. 1990 if the most recent reestablishment was post 1990. In the absence of information about the age of these forest fractions in 1990 and 2000, the fractions are assigned to old-growth forest, whereas in reality some of it might have been regrowth forest or agricultural land. Following from this, for 1981-1990 and 1991-2000, the upper and lower sensitivities for forest stand age both result in a regrowth forest area that falls below the central estimate - the lower bound of stand age results in more forest being classified as very young in 2010, and thus being assigned to old-growth forest during the earlier decades. The substantially lower uptake rate of regrowth forest during 2001-2010 is due to a large establishment of regrowth forest in the tropics during this decade, resulting in net emission in much of this region (Fig. S3). Uptake is maintained in the event that the previous land-use was cropland (orange squares) due to the recovery of carbon-depleted cropland soils.

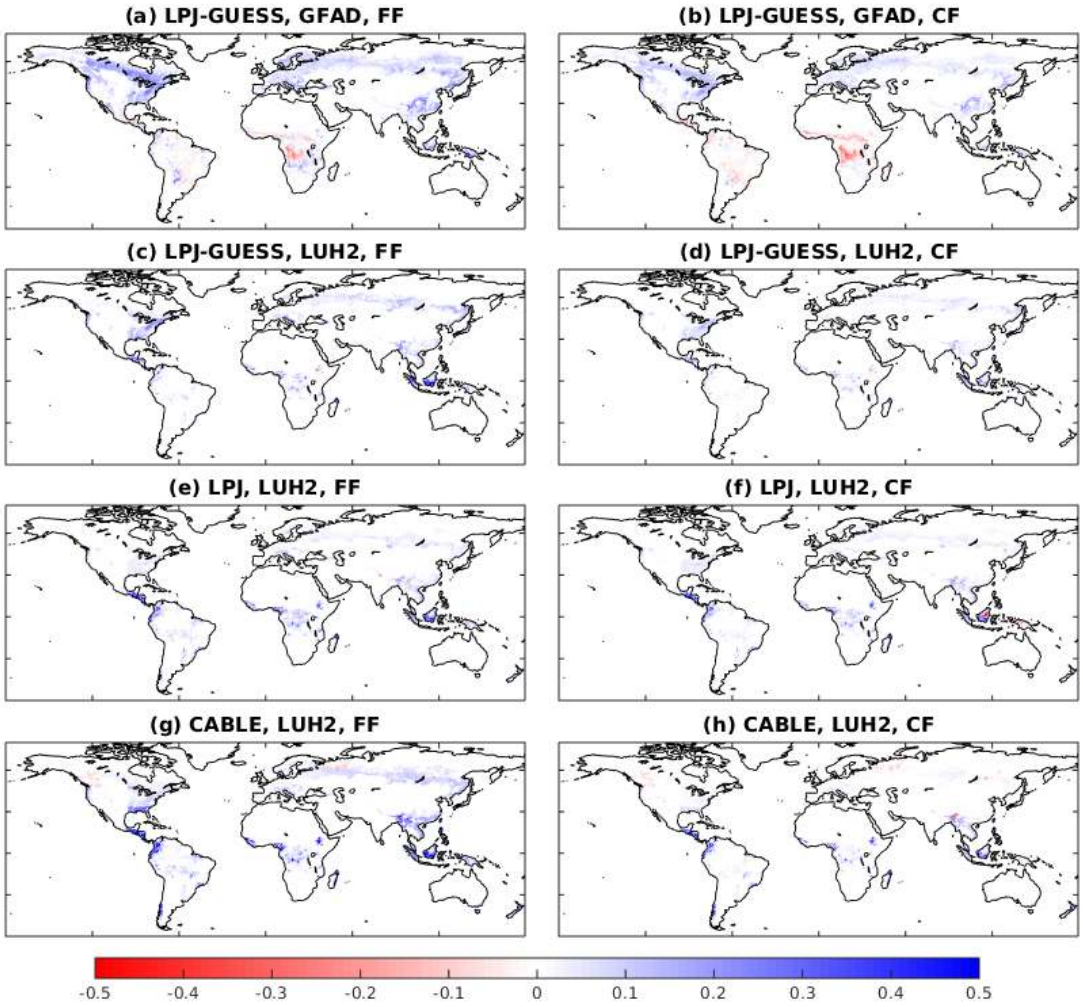

Figure S3. Maps of carbon uptake in regrowth forests (kg C m^{-2} yr^{-1}, 2001-2010 mean) as simulated by the model and forcing dataset combinations in this study. Blue shows carbon uptake and red carbon loss. Left column shows results with full environmental forcing and right column results with fixed pre-industrial forcing.

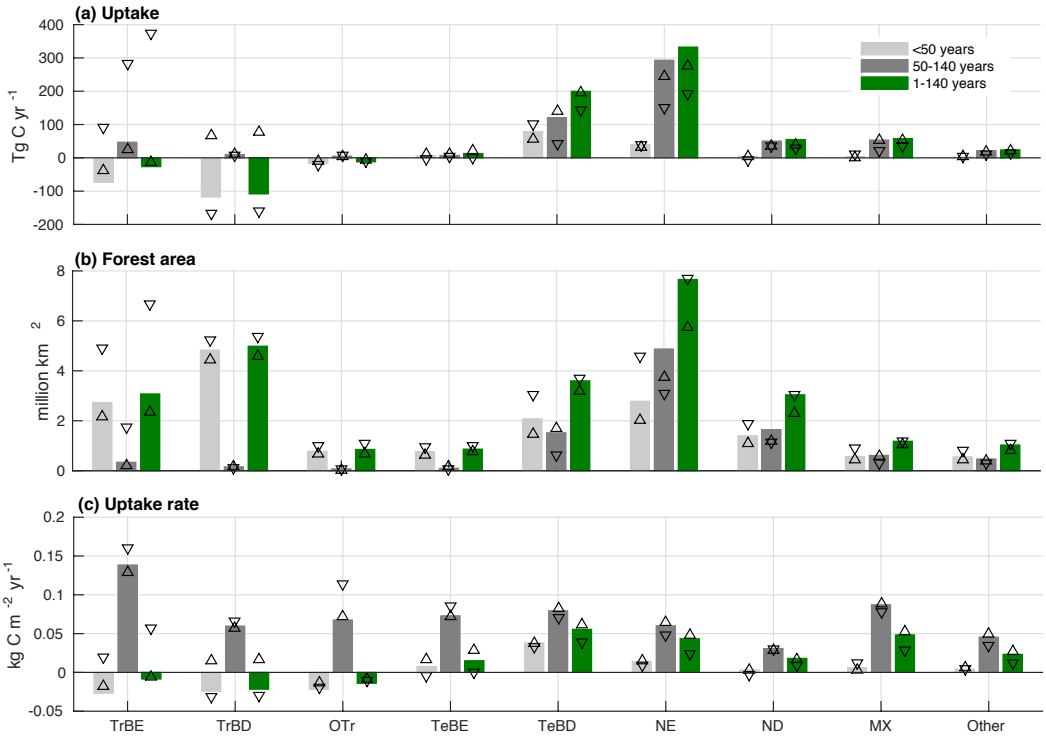

Figure S4. Contribution to regrowth sink by regrowth stand age in the CF simulation of LPJ-GUESS forced by GFAD for 2001-2010. Light grey bars show results for regrowth stands less than 50 years old, dark grey bars for stands between 50 and 140 years old, and green bars the total over 1-140 years. (a) Carbon uptake. (b) Forest area. (c) Uptake rate calculated by dividing carbon uptake by forest area for each forest type. Symbols show results from sensitivity simulations as in Fig. 2. Uncertainty becomes large for the tropical regrowth forest because much of the regrowth forest in the tropics is very young. Older regrowth stands show a pattern of carbon uptake rate that follows the relative productivity of these different forest types, whilst younger regrowth stands tend to have much lower net carbon uptake as a result of larger soil legacy fluxes and a greater fraction of stands without canopy closure.

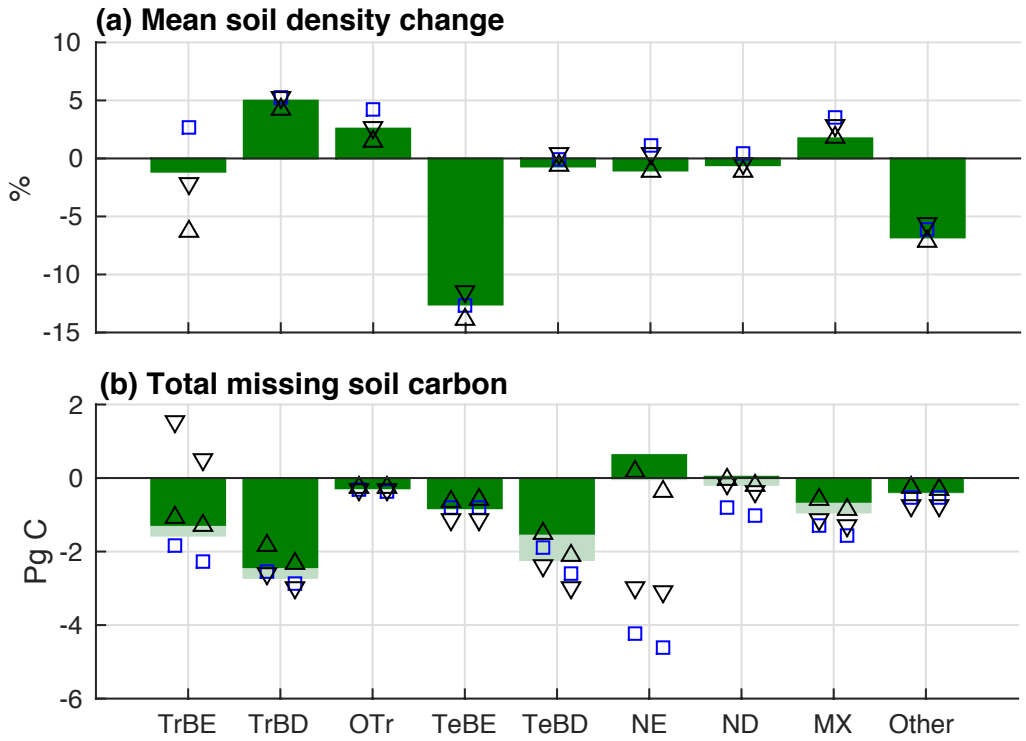

Figure S5. As for Fig. 4, but for soil and litter carbon. Note that CF and FF simulations give virtually identical results in panel b.

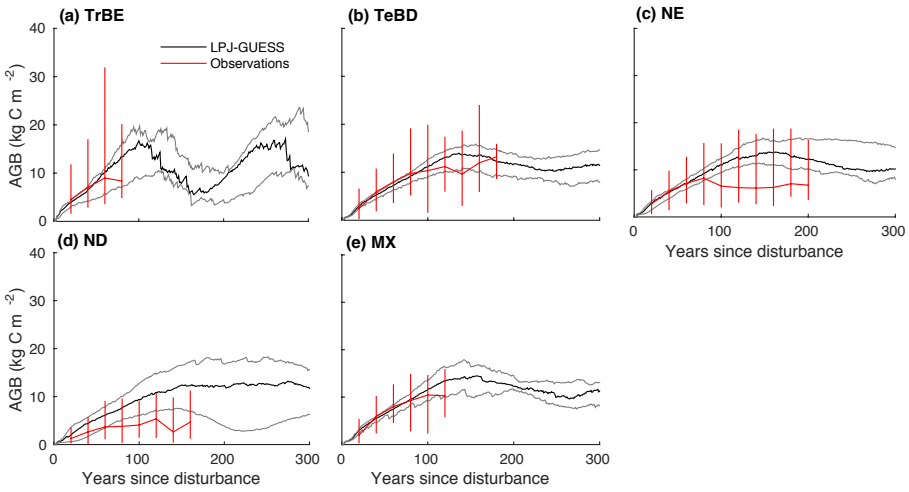

Figure S6. Comparison of biomass regrowth trajectories calculated with LPJ-GUESS with observations. The red lines are median above-ground biomass (AGB) for 20 year age bins, taken from Teobaldelli et al. (17) and Poorter et al. (18, 19) for locations within the area of that forest type. Only bins with at least 20 observations are plotted (insufficient data for TrBD and TeBE). Error bars show the 10th and 90th percentiles of the data. The median of LPJ-GUESS results for simulations at the same locations is plotted as a black line with 10th and 90th percentiles in grey. A single 0.5° x 0.5° grid cell may be represented multiple times in the average if there are multiple observations located within that cell. The simulation was 300 years under recycled, detrended, 1986-2015 climate (forcing dataset as in main text) and a fixed 2015 atmospheric CO_2 mixing ratio of 401 ppm to be appropriate for current conditions. Directly after spin-up, all grid cells were subject to stand-clearing disturbances for all patches. The vegetation was then allowed to regrow without being subject to further stand-replacing disturbances. Simulated AGB was calculated as 0.75 multiplied by the simulated total vegetation biomass to account for the below-ground fraction (20).

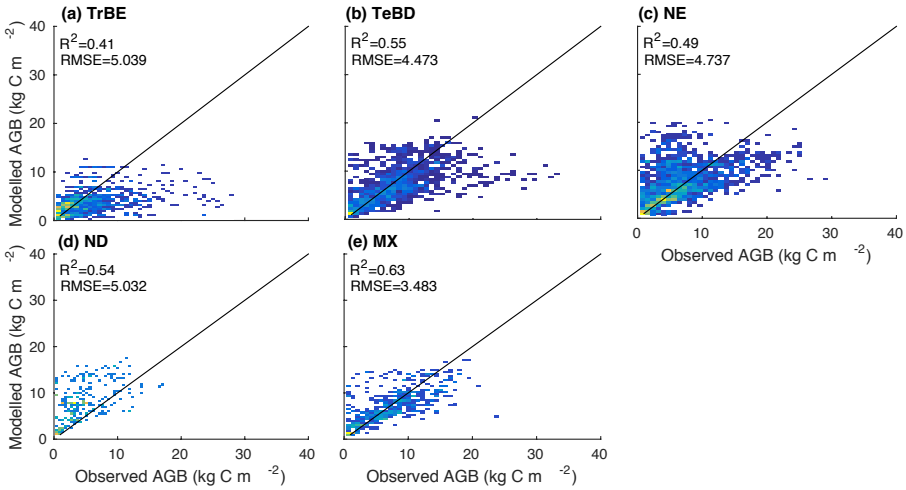

Figure S7. Comparison of observed and LPJ-GUESS simulated AGB for different forest types. Each point represents one biomass observation and age, plotted against the biomass simulated for the corresponding stand age by LPJ-GUESS. Data and simulations as described in Fig. S6. Brighter colors indicate a higher density of points.

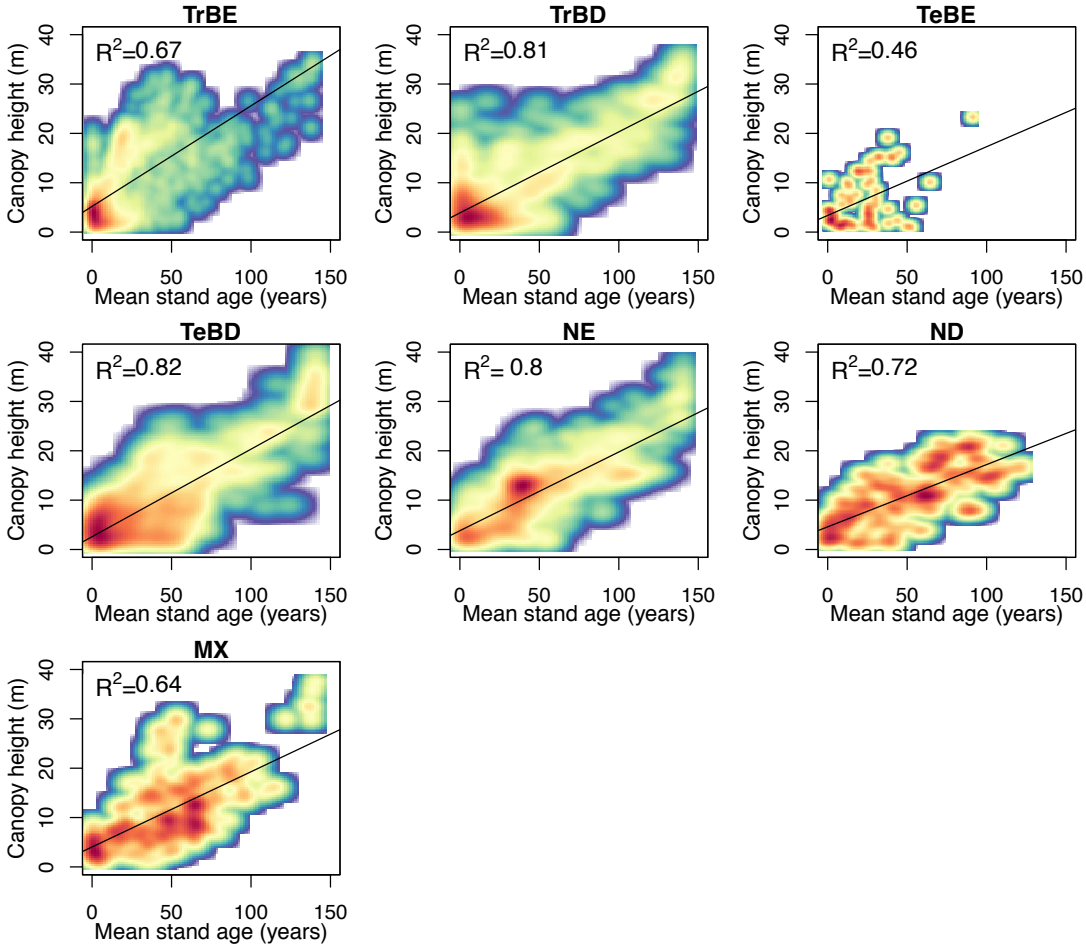

Figure S8. Relationship between GFAD mean stand age at 0.5° and mean canopy height as given by Simard et al. (21). Brighter colors indicate a higher density of points. Black lines show the best fit linear regression.

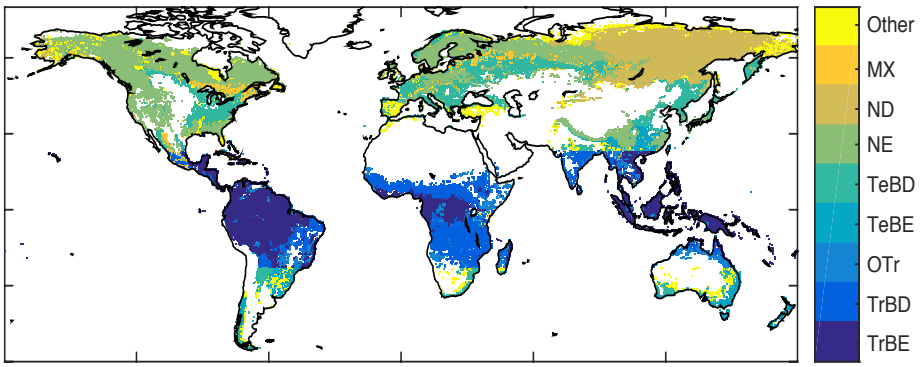

Figure S9. Locations of forest types. Only grid cells with at least 5% area classified as forest are shown for clarity.

Supporting Data

Dataset S1
ESA_forest_cover_regrowth_analysis.txt
- Raster file containing fraction forest cover per grid cell as used in this analysis.
- -99 is no data

Dataset S2
ESA_forest_9regions_regrowth_analysis.txt
- Raster file containing dominant forest type per grid cell as used in this analysis.
- Codes: 1 TrBE, 2 TrBD, 3 OTr, 4 TeBE, 5 TeBD, 6 NE, 7 ND, 8 MX, 9 Other
- -99 is no data

Supporting References

1. Poulter B, et al. (2018) *The global forest age dataset (GFADv1.0), link to NetCDF file* Available at: https://doi.pangaea.de/10.1594/PANGAEA.889943.
2. Pollard JE, et al. (2006) *Forest Inventory and Analysis National Data Quality Assessment Report for 2000 to 2003* Available at: http://www.fs.fed.us/rm/pubs/rmrs_gtr181.pdf.
3. Saatchi SS, et al. (2011) Benchmark map of forest carbon stocks in tropical regions across three continents. *Proc Natl Acad Sci* 108:9899–9904.
4. Espírito-Santo FDB, et al. (2014) Size and frequency of natural forest disturbances and the Amazon forest carbon balance. *Nat Commun* 5:3434.
5. Cole LES, Bhagwat SA, Willis KJ (2014) Recovery and resilience of tropical forests after disturbance. *Nat Commun* 5:3906.
6. Thonicke K, Venevsky S, Sitch S, Cramer W (2001) The role of fire disturbance for global vegetation dynamics: coupling fire into a Dynamic Global Vegetation Model. *Glob Ecol Biogeogr* 10(6):661–677.
7. Ellis EC, Goldewijk KK, Siebert S, Lightman D, Ramankutty N (2010) Anthropogenic transformation of the biomes, 1700 to 2000. *Glob Ecol Biogeogr* 19(5):589–606.
8. Krause A, Pugh TAM, Bayer AD, Lindeskog M, Arneth A (2016) Impacts of land-use history on the recovery of ecosystems after agricultural abandonment. *Earth Syst Dyn* 7:745–766.
9. Guo L, Gifford R (2002) Soil carbon stocks and land use change: a meta analysis. *Glob Chang Biol* 8:345–360.
10. Nyawira SS, Nabel JEMS, Don A, Brovkin V, Pongratz J (2016) Soil carbon response to land-use change: evaluation of a global vegetation model using observational meta-analyses. *Biogeosciences* 13(19):5661–5675.
11. Olin S, et al. (2015) Soil carbon management in large-scale Earth system modelling : implications for crop yields and nitrogen. *Earth Syst Dyn* 6:745–768.
12. Sitch S, et al. (2003) Evaluation of ecosystem dynamics, plant geography and terrestrial carbon cycling in the LPJ dynamic global vegetation model. *Glob Chang Biol* 9:161–185.
13. Haverd V, et al. (2013) A stand-alone tree demography and landscape structure module for Earth system models. *Geophys Res Lett* 40(19):5234–5239.
14. Haverd V, Smith B, Nieradzik LP, Briggs PR (2014) A stand-alone tree demography and landscape structure module for Earth system models: Integration with inventory data from temperate and boreal forests. *Biogeosciences* 11:4039–4055.
15. Hansis E, Davis SJ, Pongratz J (2015) Relevance of methodological choices for accounting of land use change carbon fluxes. *Global Biogeochem Cycles* 29:1230–1246.

16. Chazdon RL, et al. (2016) Carbon sequestration potential of second-growth forest regeneration in the Latin American tropics. *Sci Adv* 2:e1501639.
17. Teobaldelli M, Somogyi Z, Migliavacca M, Usoltsev VA (2009) Forest Ecology and Management Generalized functions of biomass expansion factors for conifers and broadleaved by stand age, growing stock and site index. *For Ecol Manage* 257:1004–1013.
18. Poorter L, et al. (2016) Biomass resilience of Neotropical secondary forests. *Nature* 530(7589):211–214.
19. Poorter L, et al. (2016) Data from: Biomass resilience of Neotropical secondary forests. Nature. *DRYAD*. doi:10.5061/dryad.82vr4.
20. Penman J, et al. (2003) *Good Practice Guidance for Land Use, Land-Use Change and Forestry* (Kanagawa, Japan).
21. Simard M, Pinto N, Fisher JB, Baccini A (2011) Mapping forest canopy height globally with spaceborne lidar. *J Geophys Res* 116:G04021.